# Melanoma NOS1 expression promotes dysfunctional IFN signaling

Qiuzhen Liu,[1,2] Sara Tomei,[3] Maria Libera Ascierto,[1] Valeria De Giorgi,[1] Davide Bedognetti,[1] Cuilian Dai,[4] Lorenzo Uccellini,[5] Tara Spivey,[6] Zoltan Pos,[7,8] Jaime Thomas,[1] Jennifer Reinboth,[1] Daniela Murtas,[1] Qianbing Zhang,[2] Lotfi Chouchane,[3] Geoffrey R. Weiss,[10] Craig L. Slingluff Jr.,[10] Peter P. Lee,[11] Steven A. Rosenberg,[12] Harvey Alter,[1] Kaitai Yao,[2] Ena Wang,[1,9] and Francesco M. Marincola[1,9]

[1]Infectious Disease and Immunogenetics Section (IDIS), Department of Transfusion Medicine, Clinical Center and trans-NIH Center for Human Immunology (CHI), NIH, Bethesda, Maryland, USA. [2]Cancer Research Institute, Southern Medical University, Guangzhou, China. [3]Weill Cornell Medical College in Qatar, Doha, Qatar. [4]Xiamen Heart Center, Zhongshan Hospital, Medical School of Xiamen University, Xiamen, Fujian, China. [5]Columbia University, New York, New York, USA. [6]Rush Medical School, Chicago, Illinois, USA. [7]MTA-SE "Lendület," Experimental and Translational Immunomics Research Group, Budapest, Hungary. [8]Department of Genetics, Cell and Immunobiology, Semmelweis University, Budapest, Hungary. [9]Research Branch, Sidra Medical and Research Centre, Doha, Qatar. [10]University of Virginia Health Systems, Charlottesville, Virginia, USA. [11]Cancer Immunotherapeutics and Tumor Immunology, City of Hope and Beckman Research Institute, Duarte, California, USA. [12]Surgery Branch, National Cancer Institute (NCI), Bethesda, Maryland, USA.

**In multiple forms of cancer, constitutive activation of type I IFN signaling is a critical consequence of immune surveillance against cancer; however, PBMCs isolated from cancer patients exhibit depressed STAT1 phosphorylation in response to IFN-α, suggesting IFN signaling dysfunction. Here, we demonstrated in a coculture system that melanoma cells differentially impairs the IFN-α response in PBMCs and that the inhibitory potential of a particular melanoma cell correlates with *NOS1* expression. Comparison of gene transcription and array comparative genomic hybridization (aCGH) between melanoma cells from different patients indicated that suppression of IFN-α signaling correlates with an amplification of the *NOS1* locus within segment 12q22-24. Evaluation of NOS1 levels in melanomas and IFN responsiveness of purified PBMCs from patients indicated a negative correlation between NOS1 expression in melanomas and the responsiveness of PBMCs to IFN-α. Furthermore, in an explorative study, NOS1 expression in melanoma metastases was negatively associated with patient response to adoptive T cell therapy. This study provides a link between cancer cell phenotype and IFN signal dysfunction in circulating immune cells.**

## Introduction

Patients with cancer suffer abnormalities in innate immunity exemplified by reduced phosphorylation of STAT1 by PBMCs stimulated ex vivo with IFN-α (1). Originally described in patients with advanced cutaneous melanoma (1–3), this phenomenon was subsequently documented in other cancers including colon and breast carcinoma (4). Suppression of phosphorylated STAT1 (p-STAT1) appears in stage II and deepens with disease progression. Moreover, although patients with cancer display markedly depressed levels of inducible p-STAT1 compared with those of healthy donors, dramatic differences can be observed among them, while p-STAT1 is generally inducible within a narrow range in PBMCs from normal individuals (4). These observations suggest that p-STAT1 levels in circulating cells are influenced by the biology of cancers, and this may bear clinical relevance, since inter-subject variation of p-STAT1 induced in PBMCs by treatment with high-dose IFN-α may predict clinical outcome in melanoma patients (5). Of note, in vitro response of PBMCs to IFN-α parallels the in vivo responsiveness of circulating immune cells to the same agent given systemically (6).

The mechanism leading to impairment of IFN signaling in PBMCs of patients with cancer is unknown, and a link between the genetics of a given patient's cancer and the corresponding behavior of circulating cells has not been established. Yet, if such a link could be established, PBMCs could serve as useful markers of a patient-specific tumor phenotype. This is particularly relevant, because increasing attention has been paid to the relationship between IFN signatures in the tumor immune microenvironment, the prognosis of patients with cancer (7), and/or their responsiveness to immunotherapy (8). In parallel with IFN-α signaling dysfunction in immune cells, deficiencies in IFN-α responsiveness have been documented in melanoma cell lines from patients with melanoma. Lesinski et al. (9) observed that melanoma cells respond variably to IFN-α, often exhibiting depressed JAK/STAT signaling. Interestingly, basal levels of p-STAT3 were inversely correlated with IFN-α–induced p-STAT1 (IFN-α-p-STAT1).

Here, we used a Transwell system to screen the effects of a panel of 12 melanoma cell lines on PBMCs obtained from healthy volunteers. After 7 days of coculture, we stimulated PBMCs with IFN-α. We identified two groups of cell lines that reproducibly differed in suppressing inducible p-STAT1 in PBMCs. Array comparative genomic hybridization (aCGH) pointed at a consistent amplification of 12q22-24 in cell lines with the highest immune-suppressive activity. This amplification corresponded to higher mRNA levels of *NOS1*, which is hosted within this genomic region. Functional studies corroborated the relevance of NOS1 as an inhibitor of p-STAT1 induction following IFN-α stimulation. These results suggest that NOS1 expression by melanoma cells contributes to type I IFN signaling dysfunction in cancer patients and establishes a link between the genetics of individual cancers and a circulating biomarker of potential clinical utility (Supplemental Figure 15: workflow; supplemental material available online with this article; doi:10.1172/JCI69611DS1).

**Conflict of interest:** The authors have declared that no conflict of interest exists.

**Citation for this article:** *J Clin Invest.* 2014;124(5):2147–2159. doi:10.1172/JCI69611.

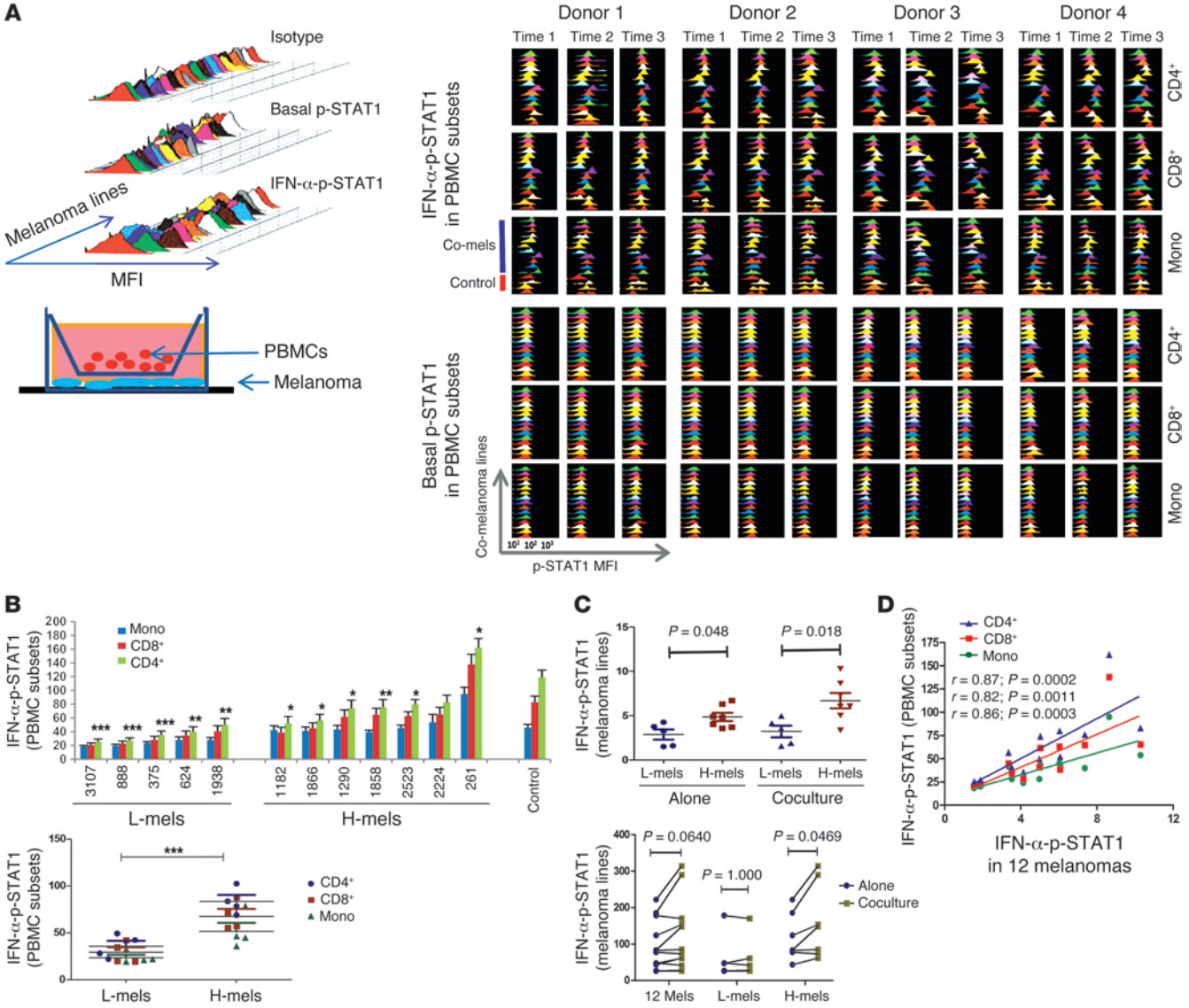


**Figure 1**

Modulation of IFN-α-p-STAT1 in PBMCs by melanoma cell lines. (**A**) Top left: Histograms of p-STAT1 levels in 25 melanoma cell lines. Isotype, basal, and IFN-α-p-STAT1 are displayed in the top, middle, and bottom panels to exemplify IFN-α-p-STAT1 variability. Bottom left: Transwell coculture of melanoma cells and PBMCs. Right: IFN-α-p-STAT1 (top) and basal p-STAT1 (bottom) in CD4+, CD8+, and monocyte subsets of PBMCs from 4 donors in triplicate experiments after a 7-day coculture with 12 melanoma cell lines (blue bar) or alone (Mono; red bar). (**B**) Top: Average IFN-α-p-STAT1 levels in CD4+, CD8+, and monocyte subsets from 4 donors cocultured with 12 melanoma cell lines or alone, as shown in **A**. Cocultured results were ranked according to IFN-α-p-STAT1 levels (*$P < 0.05$, **$P < 0.005$, and ***$P < 0.0005$, Wilcoxon test): 5 cell lines with strong inhibitory effects (reduction of IFN-α-p-STAT1 by 50% compared with PBMCs cultured alone) were determined to be L-mels, and the rest H-mels. Bottom: IFN-α-p-STAT1 in PBMC subsets cocultured with L-mels or H-mels ($P = 0.0005$, Wilcoxon test). (**C**) Top: Average IFN-α-p-STAT1 levels in L-mels before and after coculture were lower than those in H-mel cell lines (Mann-Whitney *U* test, $P = 0.048$ and 0.018) before and after coculture with PBMCs (shown for individual cell lines at the bottom). IFN-α-p-STAT1 was enhanced significantly after coculture with PBMCs only in H-mels ($P = 0.047$, Wilcoxon test). (**D**) IFN-α-p-STAT1 in melanoma cells correlated with the IFN-α-p-STAT1 in respective cocultures of CD4+, CD8+, and monocyte subsets (Spearman's correlation).

## Results

*Modulation of IFN-α-p-STAT1 in PBMCs by melanoma cell lines.* We performed flow cytometry to screen 25 cell lines for basal and IFN-α–induced (1,000 IU/ml) p-STAT1 (IFN-α-p-STAT1) levels. Consistent with previous reports (9), basal levels and response to IFN-α were heterogeneous among cell lines (Figure 1A, left), in which each cell line displayed a highly reproducible and idiosyncratic behavior. We selected 12 melanoma cell lines representative of the observed heterogeneity and tested them in a noncontact coculture Transwell system with PBMCs from healthy individuals (Figure 1A, bottom). We chose healthy donors in order to exclude any predetermined variation in PBMC response due to the cancer-bearing status. After 7 days, cell lines and PBMCs from 4 healthy donors were separated and stimulated with IFN-α (1,000 IU/ml) in three

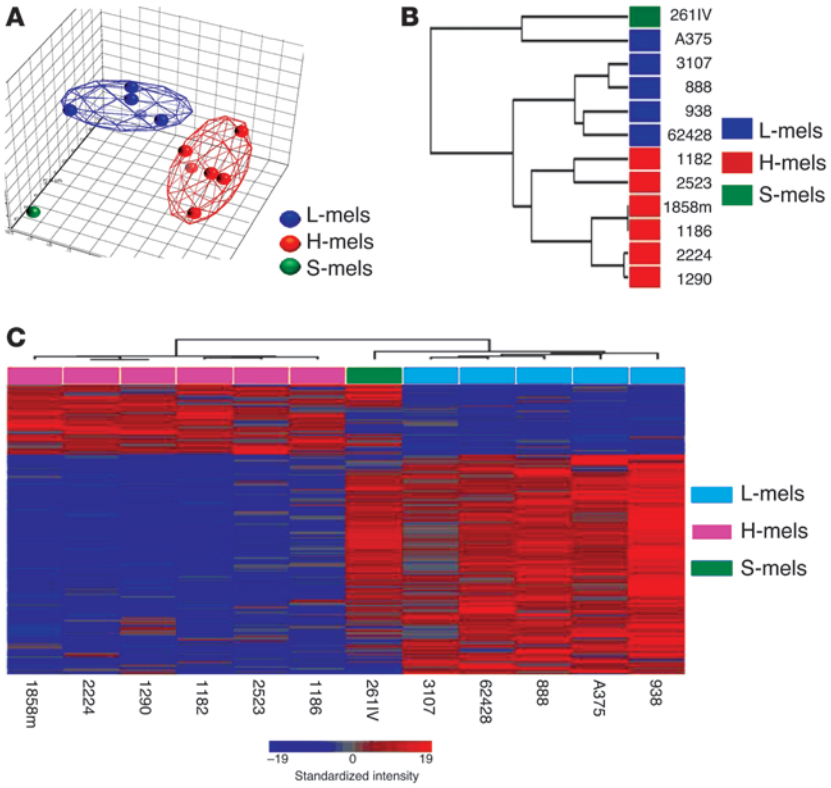


**Figure 2**
Transcriptional signatures specific for L-mels. (**A**) PCA based on global gene expression classified 12 melanoma cell lines into three groups according to immune phenotypes. (**B**) Unsupervised hierarchical clustering based on global gene expression by average linkage. (**C**) Heatmap based on 6,771 genes differentially (Student's *t* test cutoff of $P < 0.05$) expressed between L-mels and H-mels.

independent experiments. We documented the basal and IFN-α-p-STAT1 levels in the $CD4^+$ and $CD8^+$ T cells and monocyte melanoma cells (Figure 1A, right). We found that basal and IFN-α-p-STAT1 levels were highest in $CD4^+$ T cells, intermediate in $CD8^+$ T cells, and lowest in monocytes, consistent with previous reports (1, 4). Basal p-STAT1 levels in all PBMC subsets did not differ significantly between those cultured alone and those cocultured with melanoma cells, while IFN-α-p-STAT1 levels varied greatly following a cell line–specific pattern ($P$ = and 0.0001, 0.0001, and 0.0009 for $CD4^+$ and $CD8^+$ T cells and monocytes, respectively; Kruskal-Wallis ANOVA, $n = 4$) (Supplemental Figure 1). Basal p-STAT1 levels in cocultured PBMC subsets varied significantly among the 4 donors, but not IFN-α-pSTAT1 levels ($P$ = 0.0001, 0.0001, and 0.0001 for basal p-STAT1 in $CD4^+$ and $CD8^+$ T cells and monocytes, respectively, Kruskal-Wallis ANOVA, $n = 12$) (Supplemental Figure 2).

IFN-α-p-STAT1 was significantly suppressed by 10 of 12 melanoma cell lines, unaffected by one, and enhanced by another. Five cell lines suppressed IFN-α-p-STAT1 in PBMCs by more than 50% compared with that in culture alone (Figure 1B, top), resulting in significantly lower IFN-α-p-STAT1 levels in the three PBMC subsets compared with those in other cell lines ($P = 0.0005$, Wilcoxon test, $n = 12$; Figure 1B, bottom). The 5 cell lines were termed L-melanomas (further abbreviated as L-mels; lower p-STAT1 levels in corresponding PBMCs); the other 7 lines were termed H-melanomas (further abbreviated as H-mels; higher p-STAT1 levels), including the one stimulating higher IFN-α-p-STAT1 levels (individually named S-melanomas, further abbreviated as S-mels). To insure that the results were not due to the skewed generation of bovine serum–reactive T cells, we also tested the inhibitory effects of two L-mel cell lines (3107 and A375) in the presence of autologous serum in 2 healthy volunteers and observed identical results (Supplemental Figure 3). These data confirm extensive preliminary work in which various culture conditions were tested to evaluate the current Transwell method, demonstrating no significant differences when bovine serum, autologous, or serum-free medium was used. Moreover, we found that the proportion of immune cell subsets did not change significantly during these experimental conditions (Supplemental Figure 4).

L-mel cell lines cultured alone or cocultured with PBMCs displayed overall lower p-STAT1 levels than did H-mels ($P = 0.048$, and 0.018, Mann-Whitney *U* test; Figure 1C, top). In coculture, the cell lines responded to IFN-α stimulation by enhancing p-STAT1 levels; however, the enhancement reached significance only in H-mels and not in L-mels (Figure 1C, bottom). Moreover, we observed that the responsiveness to IFN-α stimulation correlated significantly with the inhibitory responsiveness of IFN-α signaling in the three PBMC subsets (Figure 1D; $P \leq 0.001$), suggesting that the same factors responsible for p-STAT1 modulation in PBMCs exert autocrine effects on melanoma cells.

*Transcriptional signatures specific for L-mels.* Principal component analysis (PCA) based on the complete Affymetrix Human Gene ST 1.0 dataset naturally segregated the 12 melanoma cell lines in L-mels versus H-mels, while S-mels clustered separately (Figure 2A). Consistently, we observed that average-linkage hierarchical clustering segregated L-mels as opposed to H-mels, while S-mels clustered separately with one of the L-mel lines (Figure 2B). Gene enrichment analysis comparing transcriptional differences between L-mels and H-mels identified 6,771 differentially expressed transcripts (ANOVA, cutoff of $P < 0.05$). Although these genes clustered S-mels together with L-mels (Figure 2C), we observed a common signature between S-mels and H-mels. The

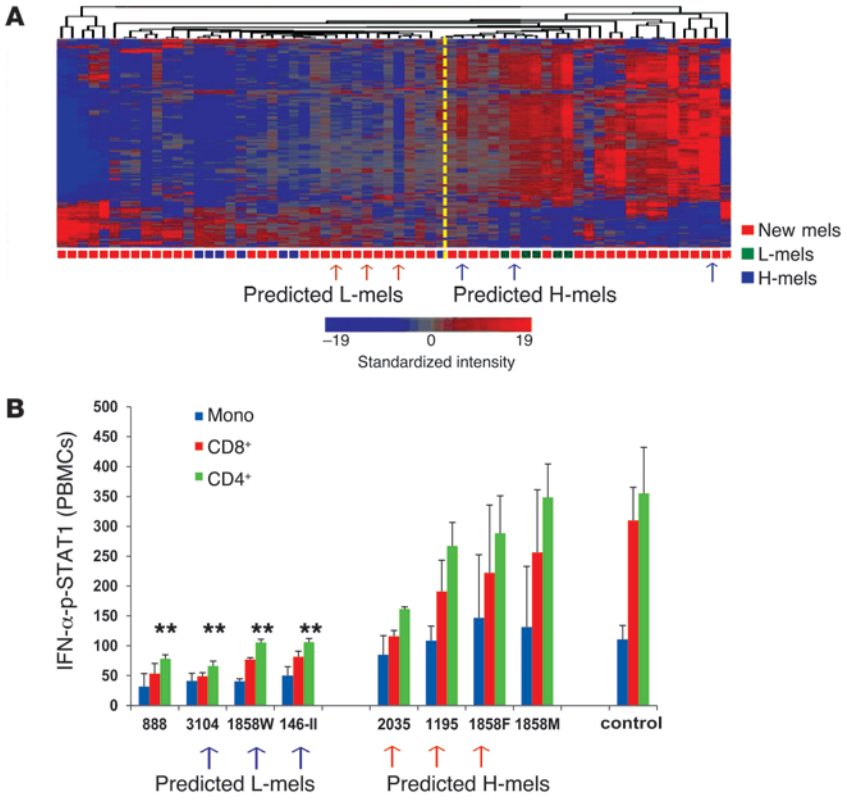


**Figure 3**
Functional validation of the L-mel signature on independent cell lines. (**A**) Heatmap based on the same genes, but including 41 additional melanoma cell lines (red) in addition to the original 12 (L-mels, green; H-mels including S-mels, blue). The 3 red and 3 blue arrows indicate 6 cell lines (3 classified as H-mels and 3 as L-mels) randomly selected for validation of the predicted modulation on PBMCs according to the 6,771 gene signatures. (**B**) The 3 lines predicted to be L-mels (blue arrows) and a previously tested L-mel (888) significantly inhibited IFN-α-p-STAT1 (Wilcoxon test, $P = 0.0039$ for all four L-mels; $^{*}P < 0.05$; $^{**}P < 0.005$; $^{***}P < 0.0005$), while the 3 new (red arrows) and the previously tested H-mels did not.

same 6,771 genes were applied to recluster 41 additional melanoma cell lines with 12 cell lines. We observed two clusters: one included the 5 L-mels and the other H-mels and S-mels (Figure 3A). We then arbitrarily selected 3 untested cell lines from each group and used the Transwell system to assess the predictive power of the gene signature differentiating L-mels from H-mels. The 3 cell lines belonging to the L group significantly inhibited IFN-α-p-STAT1 in PBMCs, while the 3 lines derived from the H group did not (Figure 3B). Ingenuity pathway analysis (IPA) based on the same gene set confirmed that the predominantly affected pathway was IFN signaling, with reduced expression of *IFNRA1*, *IFNRA2*, *JAK1*, and *JAK2* by L-mels, corresponding to inhibition of the downstream transcription IFN regulatory factors (IRFs) IRF7, IRF5, STAT1, and STAT4 (Supplemental Table 1; IPA *z* score of less than –2). In contrast, we found that the top activated pathway in L-mels was G protein–coupled receptor signaling (Figure 4), with upregulation of G protein receptors and the downstream target transcription factors HNF1A and HNF4A (Supplemental Figure 5; IPA *z* score of greater than 2), which functionally related with cellular proliferation and dependence upon STAT3 signaling. Indeed, we observed that several STAT3 target transcripts were upregulated in L-mels (Supplemental Table 2).

*12q22-24 amplification is a genomic marker for L-mel and targets the NOS1 gene*. aCGH of the 12 melanoma cell lines provided results consistent with the literature (10–13). We observed gains in chromosomes 1q, 3, 6q, 7, 8q, and 20, while losses prevailed in chromosomes 4, 6p, and 10, suggesting that both L-mels and H-mels share common genomic characteristics of melanoma. Visually, the L group consistently displayed chr12 amplification, while the H group was characterized by chr8 amplification (Figure 5A, top). Class comparison between the two groups identified ten segments that passed the one-way ANOVA cutoff threshold *P* value of less than 0.01, with a symmetrical fold change greater than 2; four of these segments were in chr8, five were in chr12, and one was in chr10 (Figure 5A, bottom).

One segment (A_14_P105868, region 950, chr12.107491693.110237959) passed the stringent cutoff of $P < 0.00001$ and overlapped with two other significantly amplified segments (A_14_P111446, region_950, chr12.107491693.110237959; and A_16_P398369, region_958, chr12.117199446-.124525018) covering a broad region of 12q22-24 (chr12:105882568-114831260) that includes 168 genes, of which 19 overlapped with the 6,771 transcripts differentiating L-mels from H-mels (Figure 5B, top, and Supplemental Table 3). Among them, HNF1A and FOX4N affect G protein–coupled receptor signaling, the top pathways engaged in the L-mel signature (Supplemental Figure 5). Moreover, the *NOS1* gene was hosted in the same region. We observed amplifications of NOS1 exclusively in L-mels, while we observed deletions only in H-mels (Figure 5B, bottom, and Supplemental Table 4). In parallel, *NOS1* mRNA expression was significantly higher in L-mels compared with that in H-mels (Figure 5C, left; $P = 0.0001$, Mann-Whitney *U* test) and correlated with NOS1 protein levels in 8 representative cell lines tested by flow cytometry ($r = 0.81$, $P = 0.032$, Spearman's coefficient; Figure 5C, right). Moreover, *NOS1* mRNA expression in the 12 melanoma cell lines correlated with suppression of IFN-α-p-STAT1 in $CD4^+$ and $CD8^+$ T cells and monocytes ($P = 0.0003$, 0.0002, and 0.0011, respectively, Spearman's coefficient; Figure 5D, left) and with their own IFN-α response ($P = 0202$; Figure 5D, right).

*Functional validation of NOS1 as a critical factor for melanoma-induced immune depression*. NOS1 synthesizes NO, which is a free radical playing a critical role in various physiological and pathological processes. To test whether NOS1 participates in melanoma-induced

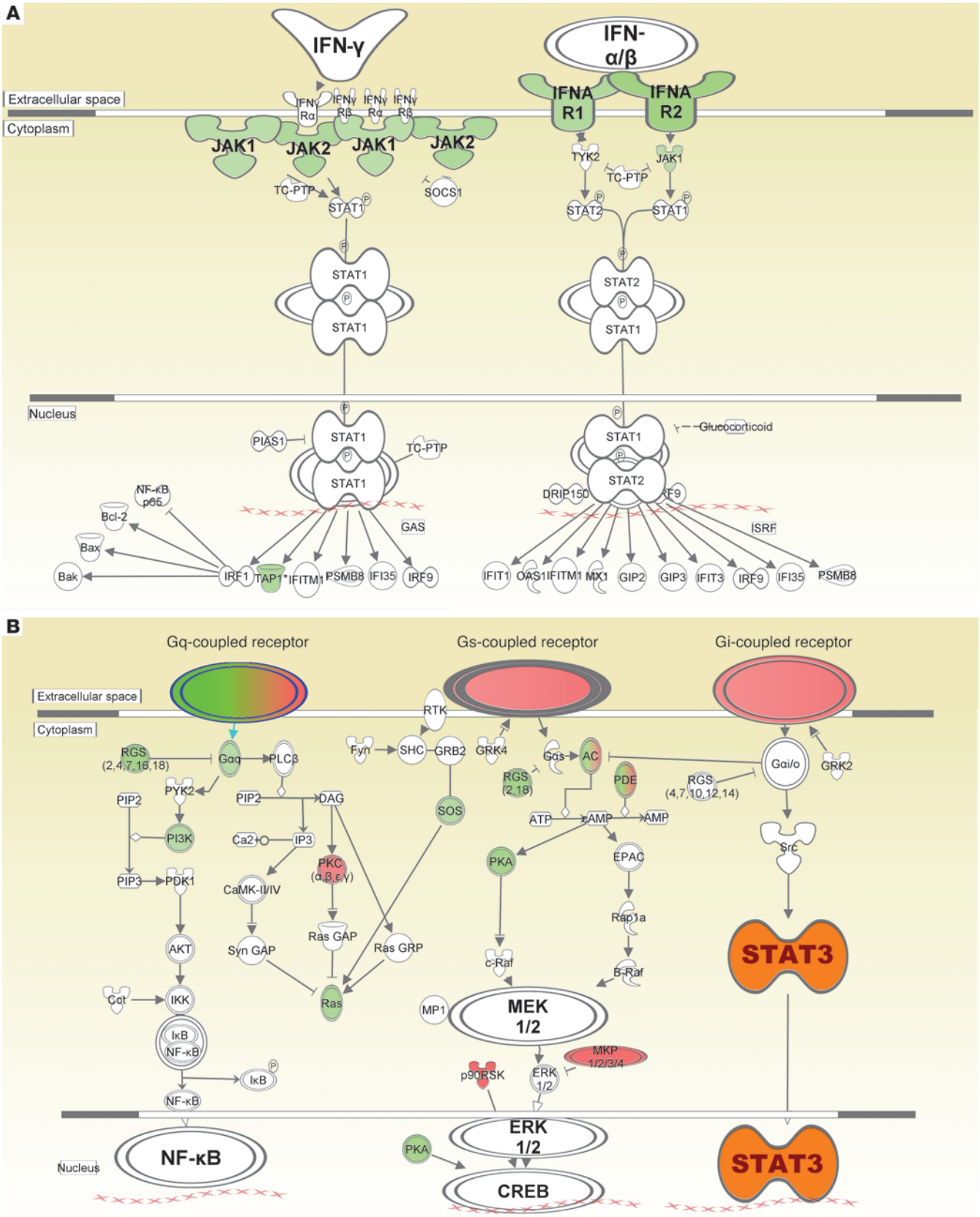


**Figure 4**

Signal pathways affected by the L-mel signature. (**A**) IFN signaling pathway according to IPA, which highlighted JAK1, JAK2, IFNA1, and IFNA2 downregulation in L-mels (green). (**B**) G-coupled receptor pathway according to IPA with receptor families. Gi-coupled receptors were upregulated in L-mels (red).

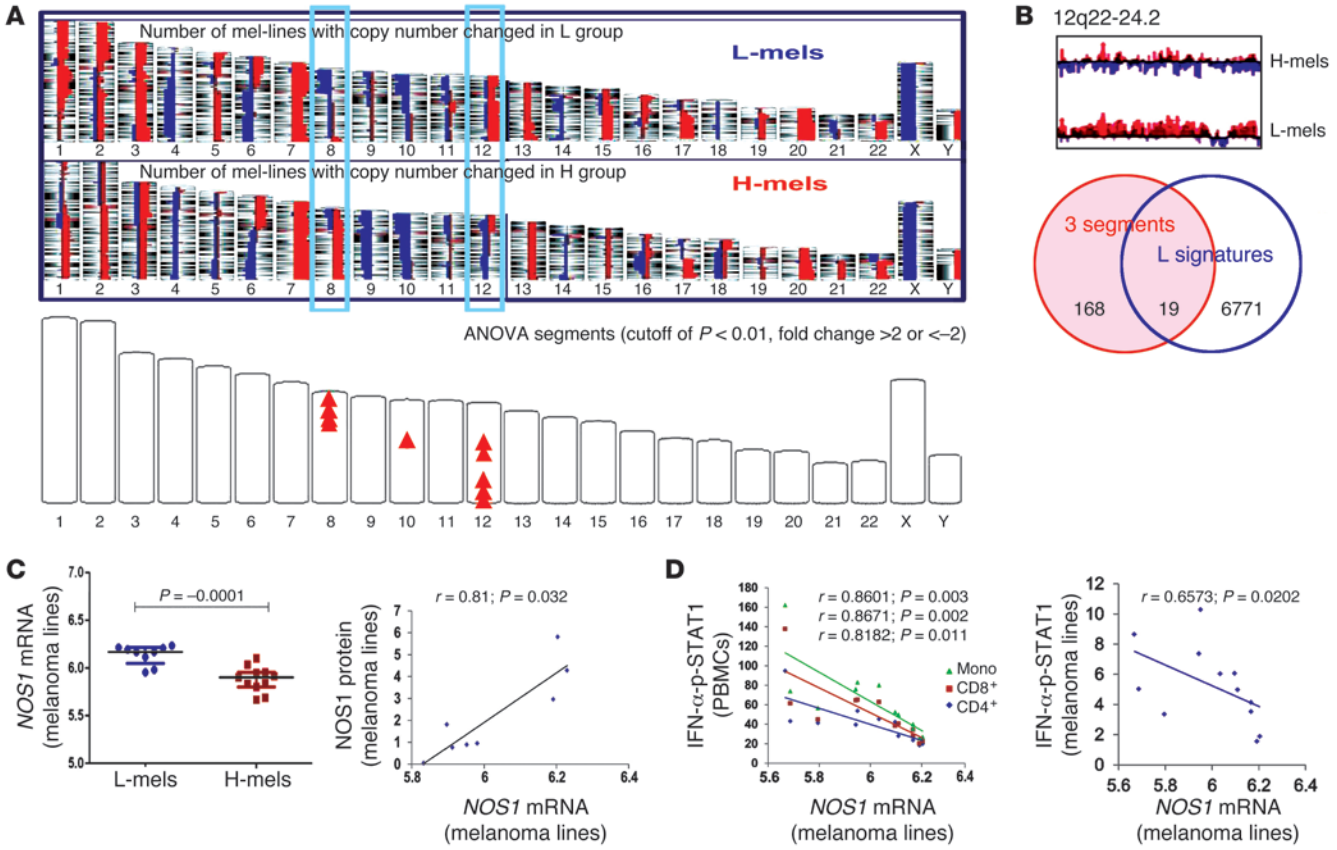


**Figure 5**

12q22-24 amplification is a genomic marker for L-mel and targets the *NOS1* gene. (**A**) Top: Chromosomal amplifications (red) and deletions (blue) in L-mels (above) and H-mels (below). Differences between L-mels and H-mels focused on chr8 and chr12 (blue squares). Bottom panel: Ten segments (red triangles) identified by ANOVA comparing L-mels with H-mels (cutoff of $P < 0.01$, fold change of less than –2 or greater than 2). The segments are located in chr8, chr10, and chr12 (4, 1, and 5 segments, respectively). (**B**) Top: Copy number values in chr12q22-24 including the most significant segment and 2 other flanking segments in which the *NOS1* gene is located (cutoff of $P < 0.00001$). Bottom: Venn diagram assembling 168 genes from 3 overlapping segments in chr12q22-24 with the 6,771 differentially expressed genes between L-mels and H-mels; 19 were in common between the two platforms, and their symbols are displayed. (**C**) Left: *NOS1* mRNA values in L-mels (blue) were higher than those in H-mels (red) ($P = 0.001$, Mann-Whitney *U* test). Right: NOS1 protein and RNA correlation in 8 melanoma lines tested by intracellular FACS analysis. (**D**) Left: Correlation between *NOS1* mRNA values in melanoma cells (*x* axis) and IFN-α-p-STAT1 levels (*y* axis) in corresponding cocultured $CD4^+$ and $CD8^+$ T cells and monocytes. Right: Correlation between *NOS1* mRNA values in melanoma cells (*x* axis) and their IFN-α-p-STAT1 levels (*y* axis). All correlation analyses in this figure are based on Spearman's correlation test.

immune suppression, we administered NONOate, a chemical product that slowly releases NO in culture and mimics NOS1 activity. NONOate induced a dose-dependent suppression of IFN-α-p-STAT1 in $CD4^+$ and $CD8^+$ T cells and monocytes ($P < 0.001$ for all concentrations tested, Wilcoxon test; Figure 6A, left). Conversely, in six independent experiments, administration of CarPITO, a scavenger of NO, caused a dose-dependent reversal of the IFN-α-p-STAT1 suppression in PBMC subsets that was induced by the three L-mels 888, 3107, and A375 ($P = 0.1173$, 0.0201, and 0.0184 at 2.5, 5, and 10 μM; Figure 6A, middle). Administration of L-NAME, a chemical inhibitor of all NOS family members (NOS1, NOS2, and NOS3), reversed the suppression induced by the three L-mels ($P = 0.3038$, 0.0169, and 0.0007 at 250, 500, and 1,000 μM; Figure 6A, right).

Selective inhibitors of NOS1 (NPLA) and NOS2 (1400W) reversed the suppression of IFN-α-p-STAT1 induced by the three L-mels at concentrations between 50 and 200 μM ($P < 0.001$ for both agents; Figure 6B), suggesting that both NOS1 and NOS2 contribute to PBMC suppression. Since monocytes present in PBMCs might be induced by melanoma cells to produce NOS2 that could indirectly contribute to p-STAT1 suppression, we cocultured purified $CD3^+$ T cells with the three L-mels. We found that $CD3^+$ T cells were also susceptible to suppression of IFN-α-p-STAT1 ($P < 0.01$), but to a significantly lesser degree than when cocultured with L-mels in the whole PBMC population ($P < 0.01$; Figure 6B, right).

Suppression of IFN-α-p-STAT1 in purified $CD3^+$ T cells was reversed by NPLA ($P = 0.0005$, 0.0006, and 0.0121 at 50, 100, 200 μM; Figure 6C, left), even at minimal concentrations of 5 μM, 10 μM, and 20 μM ($P = 0.0024$, 0.0034, and 0.0024; Supplemental Figure 6, left). In contrast, the NOS2-specific inhibitor 1400W did not significantly affect IFN-α-p-STAT1 at high or low concentrations (Figure 6C, right, and Supplemental Figure 6, right), suggesting that NOS1 is primarily responsible for suppression of IFN-α-p-STAT1 in $CD3^+$ T cells.

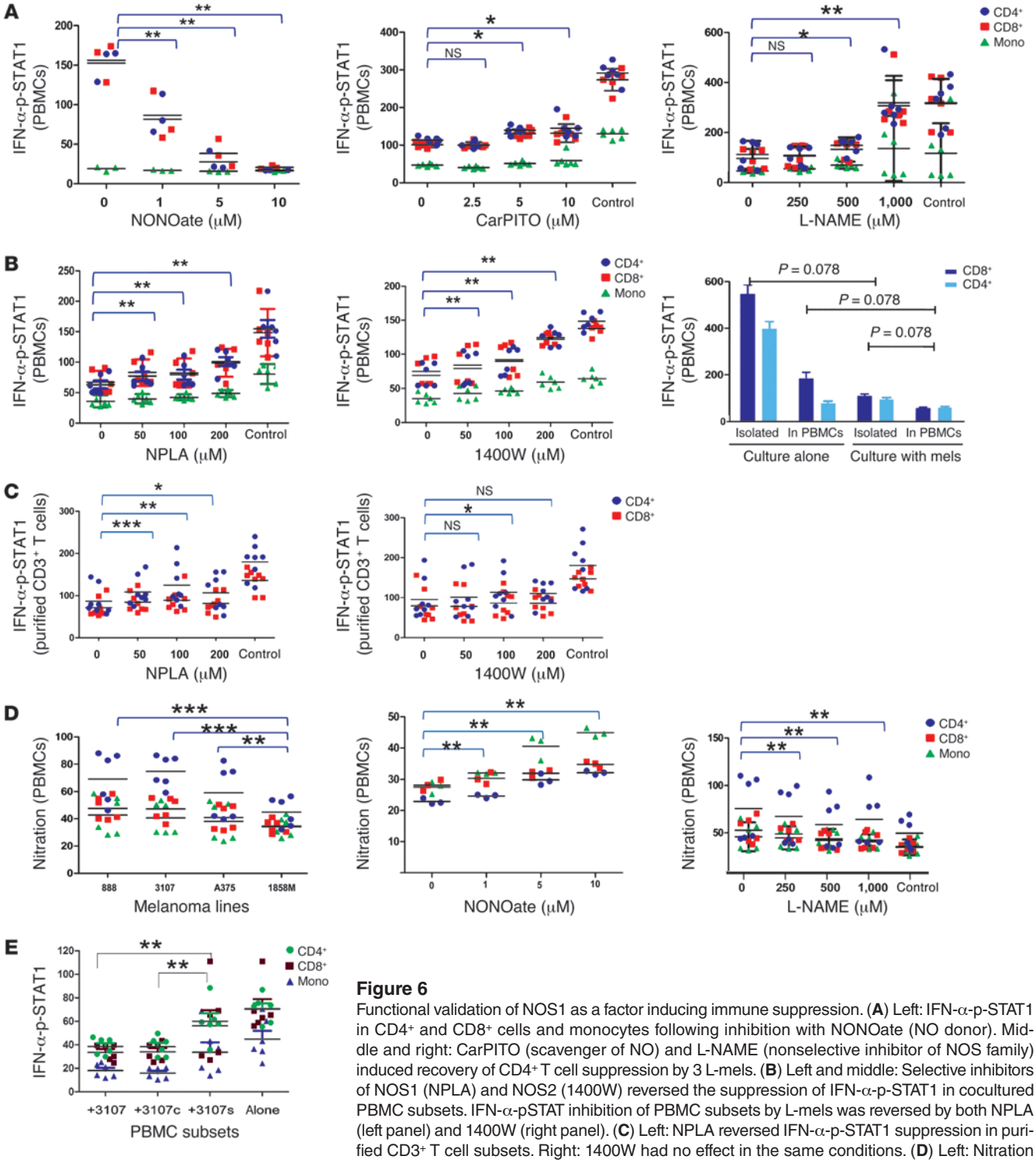


**Figure 6**

Functional validation of NOS1 as a factor inducing immune suppression. (**A**) Left: IFN-α-p-STAT1 in CD4+ and CD8+ cells and monocytes following inhibition with NONOate (NO donor). Middle and right: CarPITO (scavenger of NO) and L-NAME (nonselective inhibitor of NOS family) induced recovery of CD4+ T cell suppression by 3 L-mels. (**B**) Left and middle: Selective inhibitors of NOS1 (NPLA) and NOS2 (1400W) reversed the suppression of IFN-α-p-STAT1 in cocultured PBMC subsets. IFN-α-pSTAT inhibition of PBMC subsets by L-mels was reversed by both NPLA (left panel) and 1400W (right panel). (**C**) Left: NPLA reversed IFN-α-p-STAT1 suppression in purified CD3+ T cell subsets. Right: 1400W had no effect in the same conditions. (**D**) Left: Nitration in PBMC subsets cocultured with 3 L-mels and one with an H-mel. Middle: Nitration of PBMC subsets increased according to the NONOate concentration and was inversely correlated with IFN-α-p-STAT1. Right: Reduction of nitration in PBMC subsets by L-NAME. (**E**) *NOS1* genetic knockdown cell line 3107s significantly restored IFN-α-p-STAT1 inhibition in CD4+, CD8+, and monocyte subsets in a coculture system compared with that in parent cell line 3107 or control cell line 3107c (paired Student's *t* test, $P = 0.003$ for both 3107 and 3107c). In all experiments, the 3 L-mel cell lines used were 888, 3107, and A375, while the H-mel cell line was 1858. Data for L-mels are presented cumulatively for simplicity, although comparable results were obtained with each individual cell line. All experiments were repeated at least six times. $^{*}P < 0.05$, $^{**}P < 0.05$, and $^{***}P < 0.005$ were derived from the Wilcoxon test or Spearman's correlation.

Nitrotyrosine is considered a marker of NO-dependent redox activity and parallels NO levels. We observed that nitration levels were significantly higher in $CD4^+$ and $CD8^+$ T cells and monocytes cultured with L-mels (888, 3107, and A375-MEL) compared with those seen in H-mels (1858-MEL) ($P = 0.0003$, 0.0003, and 0.0017 for 888, 3107, and A375-MEL) and were negatively correlated with the corresponding IFN-α-p-STAT1 levels in PBMC subsets ($P < 0.0001$, Spearman's correlation; Figure 6D, left). We found that nitration levels were enhanced in PBMCs according to the dosage administration of NONOate ($P = 0.0039$, 0.0039, and 0.0039 for 250, 500, and 1,000 μM) and inversely correlated with IFN-α-p-STAT levels ($P = 0.0001$; Figure 6D, middle), while they were reduced by L-NAME ($P = 0.0015$, 0.0009, and 0.00102 for 250, 500, and 1,000 μM,) and inversely correlated with IFN-α-p-STAT1 levels ($P = 0.0031$; Figure 6D, right).

To further assess the role of NOS1 in suppressing IFN-α-p-STAT1, we applied genetic knockdown technology to the strongly inhibitory L-mel 3107 cell line (Figure 6E). We found that the levels of IFN-α-p-STAT1 were significantly restored in $CD4^+$, $CD8^+$, and monocyte subsets pretreated with shRNA (3107s), but not shRNA control (3107c).

*Correlation between NOS1 expression by metastatic melanoma and responsiveness of circulating PBMCs to IFN-α stimulation ex vivo*. Simultaneously collected metastatic melanoma samples and PBMCs from 9 patients were tested by global transcriptional profiling (14). Canonical modulators of IFN-α signaling such as IFNAR2, JAK1, STAT1, IRF7, and IRF1 were downregulated in the metastases and PBMCs compared with the reference PBMCs from healthy individuals, while IRF2 and STAT3 were upregulated (Figure 7A, left and middle). The degree of deregulation of these factors was highly correlated between melanoma and corresponding PBMCs (Pearson's $P = 0.0001$, $n = 63$; Figure 7A, right).

We also tested 8 available cryopreserved PBMC samples from the 9 patients for p-STAT1, p-STAT3, and p-IRF7 before and after IFN-α stimulation (1,000 IU/ml). Both basal and IFN-α-p-STAT1 levels trended toward an inverse correlation with NOS1 expression in melanomas, with IFN-α-p-STAT1 being significantly affected in $CD8^+$ T cells ($P = 0.0078$, Figure 7B, left). We found that basal and IFN-α-p-STAT3 did not correlate significantly (not shown); however p-STAT3/p-STAT1 ratios were positively correlated with NOS1 expression in $CD4^+$ T cells in tumors ($P = 0.0242$, Figure 7B, middle). Moreover, basal IRF7 levels in PBMCs did not vary, while IFN-α-pIRF7 inversely correlated with tumor NOS1 expression in all subsets and significantly so in $CD8^+$ T cells (Figure 7B, right). Interestingly, the correlation between NOS expression and IFN-α-p-STAT1 in monocytes was quite modest. Therefore, in PBMC subsets obtained ex vivo, we evaluated the correlation between IFN-α–induced STAT1 with in vivo NOS2 expression by paired melanoma metastases. Surprisingly, NOS2 expression did not correlate with IFN-α-p-STAT1 in $CD4^+$ and $CD8^+$ subsets, but it was positively correlated in monocytes (Pearson's $r$; $P = 0.0706$, 0, 0.0926, and 0.0091; Supplemental Figure 7, left). We found no correlation between NOS2 expression and IFN-α-p-STAT3/1 or IRF7 in any of the three subsets ($P = 0.1044$, 0.5197, and 0.6175 for IFN-α-p-STAT3/1; $P = 0.4597$, 0.6657, and 0.2282 for IRF7 by $CD4^+$, $CD8^+$, and monocyte subsets, respectively; Supplemental Figure 7, middle and right), suggesting that regulation of STAT activation is multifactorial in vivo and that NOS1-PBMC interactions in vitro indicate a significant, but not unique, contribution by cancer cells to the regulation of immune activation in vivo.

*NOS1 expression by melanoma metastases is associated with immune responsiveness to adoptive T cell transfer therapy*. We evaluated the relationship between NOS1 expression and responsiveness to immunotherapy in 113 melanoma metastases excised for the expansion of tumor-infiltrating lymphocytes (TILs) to be adoptively transferred (15, 16). Of the 113 patients, 24 experienced a complete response (CR), 35 had a partial response (PR), and 54 had no response (NR) according to the response evaluation criteria in solid tumors (RECIST).

The distribution of NOS1 expression values in the 113 metastases was bimodal ($P < 0.01$, Kolmogorov-Smirnov normality test) and naturally ranked the 113 cases into high- and low-expression groups according to a mean NOS1 expression of 4.4 (Figure 7C, left). The high-expression NOS1 group ($n = 56$) was enriched with NR (CR + PR versus NR = 6 + 16 versus 34, $n = 56$) compared with the low-expression group (CR + PR versus NR = 18 + 19 versus 20, $n = 57$) ($P = 0.011$, $\chi^2$ test). NOS1 expression was inversely correlated with therapeutic outcome ($P = 0.0001$, Spearman's coefficient rank correlation; Figure 7C, right). NOS1 expression was lower in CR patients, intermediate in PR patients, and higher in NR patients (mean ± SEM: 4.22 ± 0.04433, 4.333 ± 0.0432, and 4.454 ± 0.0420 for CR, PR, and NR patients, respectively; $P = 0.0003$, one-way ANOVA; Figure 7D, left), and NOS1 expression in CR plus PR patients (overall response, OR) differed from that observed in NR patients ($P = 0.0002$; Figure 7D, right). In contrast, we found that the expression of NOS2 and NOS3 in 113 metastases was normally distributed and did not correlate with therapeutic outcome (Supplemental Figure 8). However, NOS1 expression correlated with NOS2 and NOS3 ($r = 0.5616$, $P < 0.0001$, and $r = 0.308$, $P < 0.0001$ for NOS2 and NOS3; Supplemental Figure 9). Hierarchical clustering based on NOS1, NOS2, and NOS3 expression values segregated the 113 cases into three groups: one with coordinated high expression of all *NOS* genes and enriched with NRs, another with low expression enriched with CR, and a third with discordant expression of NOS genes corresponding to a mixture of CRs, PRs, and NRs (Figure 7E).

## Discussion

This study suggests that NOS1 expression links immune dysfunction in circulating immune cells with a genetically identifiable phenotype of melanoma. We documented that NO produced by NOS1-expressing melanoma cells directly inhibits IFN-α signaling in PBMCs in a coculture system and acts as an initiator of the expression of other *NOS* genes in the presence of other immune cells. It should be noted that since we used the Transwell system, we could not exclude a priori an additional potential role of pathways activated by cell-to-cell interactions and, therefore, the in vitro culture system might not entirely reflect the in vivo situation. In particular, the relationship between NOS1 expression and activation of STAT1 is exclusive only when observed in vivo, suggesting that this mechanism can independently, but not exclusively, affect the immune activation status in vivo. Other factors may contribute to this, as suggested by the healthy expression of NOS2 and NOS3 in vivo (Supplemental Figures 7 and 8). We would like to emphasize that this study was primarily aimed at understanding the relationship between cancer genotype and STAT1 activation potential in circulating cells. Our assessment of associations between NOS expression and cancer phenotype and clinical outcome produced secondary interpretations about the potential relevance of these findings to the tumor microenvironment. But these

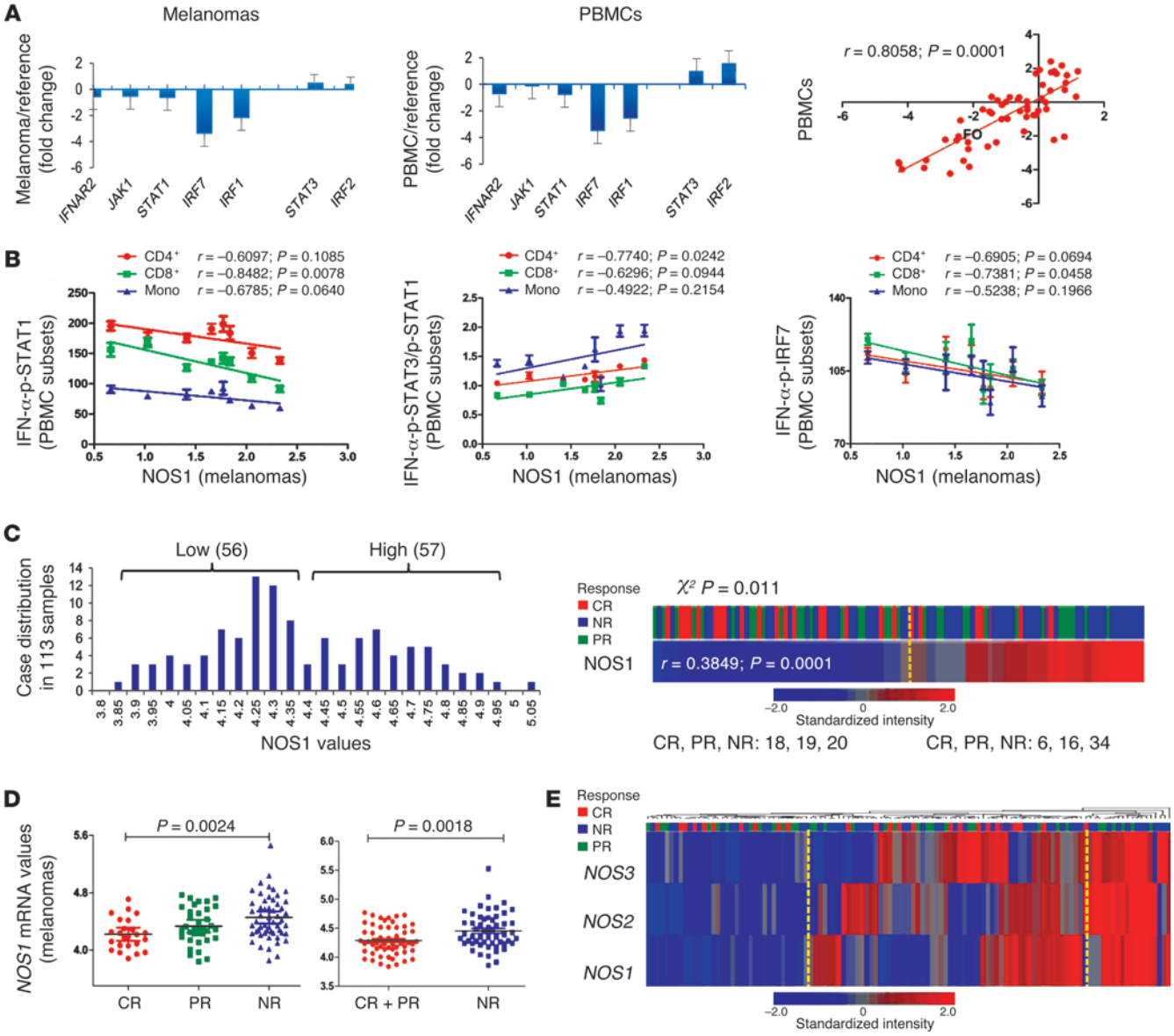


**Figure 7**

NOS1 expression by melanoma metastases. (**A**) mRNA levels of IFN-α–related signaling genes in 9 melanoma metastases (left) and simultaneously collected autologous PBMCs (middle) presented as fold change compared with healthy donors' PBMCs. Right: Scatter plot displaying correlative values for transcripts shown in the previous two panels comparing melanoma metastases (*y* axis) and PBMCs (*x* axis); $n = 63$. (**B**) Scatter plots correlating ex vivo IFN-α-p-STAT1 (left), IFN-α-p-STAT3/p-STAT1 (middle), and IFN-α-pIRF7 (right) with NOS1 expression in 8 available PBMCs (*y* axis). (**C**) Left: lack of normal distribution of NOS1 expression in melanoma metastases ($P < 0.01$, Kolmogorov-Smirnov normality test) and ranking of the 113 cases into high- and low-expression groups according to the mean NOS1 expression value (4.40). Right: NOS1 expression in melanoma was inversely correlated with therapeutic outcome (Spearman's rank correlation coefficient). The high-expression NOS1 group was significantly enriched with NR cases ($P = 0.011$, $\chi^2$ test); (**D**) Left: *NOS1* expression in 113 melanoma metastases from patients receiving adoptive TIL therapy segregated according to response to therapy (CR, PR, and NR; *P* values refer to one-way ANOVA). Right: *NOS1* expression in overall response (CR + PR) compared with NR cases (unpaired Student's *t* test). (**E**) Hierarchical clustering of the 113 metastases according to NOS1, NOS2, and NOS3 displaying three groups, one with concordantly high expression of the 3 NOS genes and enriched in NRs, the other with low expression, and the third with discordant expression. All correlative analyses are based on Pearson's correlation test.

should be viewed as preliminary and explorative observations to direct future studies. Similarly, the role of NOS1 as a potentially predictive biomarker of immune responsiveness to adoptive T cell therapy should be seen only as explorative, since no prospective validation could be entertained by this purely mechanistic study.

Nevertheless, these findings suggest that melanoma cell–derived NO is a crucial modulator of immune function in the tumor microenvironment and provides a potentially novel target for immunotherapy. It should be emphasized that the relationship between activation of STAT1 in circulating PBMCs and the

cancer-bearing status was observed exclusively from stage II, and it was most prominent after stage III. This study, therefore, assessed the relationship between cancer genotype and STAT1 activation in circulating cells at the later stages. We cannot conclude that the information obtained could also be extrapolated to the early phases of tumor/immune cell interactions in the microenvironment of primary tumors.

There has been growing interest in a reclassification of cancer based on immunologic parameters (8, 17). Although the weight that cellular immune infiltrates bear on the natural history of melanoma has been long known (18, 19), this observation was recently characterized in greater detail and expanded to other cancer types (7, 20, 21). In particular, it has been shown that the type and function of immune infiltrates and the immune texture in which they present bear prognostic power beyond the classic tumor, node, metastasis (TNM) staging (7), which does not take into account specific immunologic signatures (22). This relationship between immune phenotype and prognostic connotation pertains to most cancers (8) and is predictive of the responsiveness of cancer to immunotherapy (8, 23–25). While a worldwide effort is currently being made to validate the observation at multinational and multiinstitutional levels, work is also being done to identify (a) genetic determinants that could explain the cancer phenotypes and (b) biomarkers detectable in the peripheral circulation that could be linked to this prognostic phenotype thus far identifiable only in excised tumor tissue.

Parallel with and separate from these efforts are attempts by others to characterize the immune phenotype of cancer patients by evaluating the immunologic characteristics of circulating immune cells (1, 3, 4, 26–32). Among the various markers of immune dysfunction associated with cancer-bearing status, the level of IFN-α-pSTAT1 in PBMCs was a reproducible parameter that was first documented in melanoma patients (1, 3, 28) and subsequently in patients with breast and colon cancer (4).

Although variation in IFN-α-p-STAT1 in PBMCs might be related to individual genetic characteristics that could predispose to the development of cancer, we believe that such dysfunction is primarily due to the cancer-bearing status for two reasons: (a) such variation is not observed in normal healthy individuals (of whom a proportion will eventually develop cancer); and (b) the alterations appear after stage II and worsen along with disease progression (4). It is important to note that although average patients with cancer experience a significant stage-dependent decrease in IFN-α-p-STAT1 compared with healthy individuals, a wide variation is observed among them, with some patients maintaining a normal pattern of responsiveness even at a late stage. The latter observation suggests that individual cancers may have distinct effects on circulating cells, perhaps through the release of immune regulatory factors. Here, we related phenotypic and genetic characteristics of melanoma cells with their effects on PBMCs in an in vitro model. We elected to test the effect of melanoma cells on PBMCs obtained from normal healthy volunteers to avoid confounding factors related to intrinsic genetic or acquired determinants of PBMC behavior in cancer patients, therefore testing exclusively whether cancer cells can determine immune dysfunction. We used cell lines belonging to a collection that was expanded from melanoma metastases at the Surgery Branch of the NCI and extensively characterized according to their genotype and phenotype (13, 33, 34).

The current study, based on an in vitro Transwell system, provides a few insights about determinants of immune dysfunction in PBMCs: (a) altered IFN-α-p-STAT1 is at least in part dependent upon soluble factors released by cancer cells; (b) this effect is idiosyncratic, as cancer cells displaying the strongest immune suppressive activity also displayed a distinct phenotype both at the functional (decreased IFN-α-p-STAT1, Figure 1C) and transcriptional levels (Figure 2); (c) the idiosyncratic behavior could be tied to specific genetic characteristics of the melanoma cell lines. Copy number analysis identified 12q22-24 amplification as a genomic marker of the immunosuppressive phenotype (Figure 5); (d) the genomic imbalances associated with the immune suppressive phenotype pointed to NOS1 as a factor for melanoma-induced immune suppression (Figure 5). NOS1 expression was validated in vitro as a determinant of immune cell dysfunction (Figure 6); (e) a relationship was established in vivo between NOS1 expression in tumors and immune dysfunction of circulating immune cells (Figure 7, A and B); (f) the link between NOS1 expression by cancer tissues and immune dysfunction of circulating cells could be expanded to a broader interpretation of a poor prognosis cancer phenotype that we recently described as being characterized by an enrichment of Th17 signatures, activation of WNT signaling, and decreased responsiveness to adoptive T cell immunotherapy; indeed, NOS1 expression was strongly enhanced in melanoma metastases bearing this phenotype (Supplemental Figure 10 and ref. 13). It is unclear whether the postulated systemic effects promoted by NOS1 secretion by tumors sufficiently alter the function of nonantigen-specific T cells to indirectly affect the migration of immune cells, including those relevant to cancer rejection, by a general mechanism of immune suppression. This is a likely possibility, considering the depletion of Th1 signatures and the low expression levels of *CD4* and *CD8* mRNA in NOS1-expressing tumors according to a previously described characterization of melanoma metastases (13); (g) NOS1 expression by tumor tissues also appeared to be related to immune responsiveness to adoptive TIL therapy (Figure 7, C and D), and an inverse correlation was observed between NOS1 expression by metastases and IFN-α-p-STAT3/p-STAT1 and p-STAT3 levels (another important marker of cancer immune dysfunction) (9, 35–39). It should also be emphasized that this study focused on cancer genotypes likely to initiate immune suppression, while other mechanisms mediated by a bystander immune suppressive mechanism such as myeloid-derived suppressor cells or tumor-derived mesenchymal stem cells may further modify the effects of cancer cells within the tumor microenvironment. This is suggested by experiments showing that purified T cell subsets lacking other suppressive mechanisms could still be inhibited by L-mels. This effect could be reversed only by the NOS1 selective inhibitor NPLA, but not by the NOS2 inhibitor 1400W. When T cells were mixed with monocytes, the T cell inhibition was stronger. Furthermore, the NOS2-specific inhibitor 1400W partially reversed the inhibition (Figure 4). Thus, melanoma-generated NOS1 might be critical in vivo for cancer-related immune suppression, and NOS2 produced by monocyte subsets, including MDSCs, amplified the inhibitory function of L-mels through the NOS1 product as a secondary, yet important, mechanism.

An interesting observation was the predominant effect of NOS1 expression on immune dysfunction compared with the current focus of the literature on NOS2 (inducible NOS) as an in vivo marker of immune dysfunction in breast and prostate cancer (40, 41). This discrepancy could be explained in two ways. First, melanoma derives from melanocytes that are neuroectodermal

cells, and NOS1 is generally expressed by such lineage; thus, a lineage-specific bias may explain this finding. Second, the in vitro model suggests that NOS2 participates in the immune suppressive activity through activation of the monocyte population in PBMCs (Figure 6). This also corresponded with a correlation we observed in vivo among 113 melanoma cases, in which NOS1 and NOS2 appeared to be coexpressed, whereas such a correlation was not observed in pure melanoma cells cultured in vitro (data not shown). Thus, our observation suggests that, at least in melanoma, NOS1 takes the driver's seat to induce immune suppression, which is subsequently amplified by inducible NOS (NOS2).

In summary, this study provides a possible link between some of the genetic and phenotypic characteristics of cancer cells and the immune alterations observable in the peripheral circulation. This link provides prognostic and predictive implications for following the natural course of cancer progression.

## Methods

*Cell lines and cell culture*. Melanoma cell lines expanded from melanoma metastases at the Surgery Branch of the NCI and extensively characterized (13, 33, 34) were maintained at 37°C in complete medium (RPMI 1640 with 10% FCS, 2 mM L-glutamine, 100 U/ml penicillin, and 100 μg/ml streptomycin) in humidified 5% $CO_2$ incubators and passaged twice per week by trypsinization.

PBMCs were collected from healthy blood donors at the Department of Transfusion Medicine, Clinical Center, NIH, isolated by density gradient separation (Ficoll-Hypaque; Sigma-Aldrich), and stored at –80°C. $CD3^+$ T cells were isolated by a Pan T cell isolation kit II (Miltenyi Biotec) through an autoMACS Separator (Miltenyi Biotec). For coculture, $5 \times 10^4$ melanoma cells were seeded in 6-well plates with 2 ml medium overnight. The Transwell was then inserted (BD Falcon TM inserts), and $2 \times 10^5$ thawed PBMCs were added. The Transwells were kept in the incubator for 7 days before testing. Day 7 was chosen based on the optimal distribution of p-STAT1 variance detected in preliminary time course studies demonstrating that suppression occurred after day 5 and reached a plateau on day 9 (Supplemental Figure 11). The chemicals NPLA, DETA NONOate (Cayman Chemical), CarPITO, L-NAME, and 1400W (Sigma-Aldrich) were stored in DMSO and dissolved in medium for immediate use.

*Cell staining and flow cytometric analysis*. Phosphorylation assays were performed as previously described (42). PBMCs were harvested into two tubes at 37°C; the one for basal p-STAT1 assessment was immediately fixed in 3% PFA for 30 minutes, and the other was kept at 37°C while stimulated with 1,000 U/ml IFN-α-2b (R&D Systems) for 23 minutes and then fixed in PFA. Permeabilization was performed with 100% methanol at –20°C overnight. Melanoma cells were harvested using the nonprotolytic cell detachment solution Detachin (Genlantis) and treated in the same manner as the PBMCs. Phosphorylation staining was done using antibodies against p-STAT1 (Tyr701) Alexa Fluor 647, p-STAT3 (Tyr705) PE, p-IRF7 (p-S477/p-S479) Alexa Fluor 647, and antibodies against CD4-FITC, CD3-PerCp, STAT1-PE, STAT3-APC, and IRF7-PE (all from BD Biosciences) after titration by incubation for 1.5 hours at room temperature. Samples were then washed and tested by flow cytometry (BD FACSCalibur). Data were analyzed by FlowJo software (Tree Star Inc.). IFN-α-p-STAT1, basal p-STAT1, p-STAT3, and p-IRF7 levels in PBMCs were calculated as the mean fluorescence of phosphorylated markers. For melanoma cells, IFN-α-p-STAT1 was assessed as fold change $F_{IFN\text{-}\alpha}/F_{basal}$, where $F_{IFN\text{-}\alpha}$ and $F_{basal}$ represent the mean fluorescence of p-STAT1 in the presence or absence of stimulation, since basal p-STAT1 levels varied among melanoma cell lines. For the NOS1 expression assay, NOS1 mAb (Epitomics, Abcam) was diluted 1:400, incubated at 4°C overnight, and followed by a second antibody staining with Dye 670 rabbit anti-mouse (1:400, 3068-1; EPITOMICS). For the nitrotyrosine assay, antinitrotyrosine antibody (Millipore) was added according to the manufacturer's instructions and incubated at 4°C overnight.

*RNA interference*. To inhibit the efficiency of human NOS1 expression in the 7-day coculture system, we used the shRNA expression constructs HSH011865-HIVmH1 and control chRNA (GeneCopoeia). Stable cell lines expressing shRNA or chRNA were selected by puromycin. Western blot and quantitative PCR (qPCR) analysis were performed to measure the knockdown efficacy in the melanoma cell line 3107 according to the percentage of reduction in mRNA expression, comparing shRNA with control (Supplemental Figures 12–14). For qPCR analysis, total RNA was isolated from cultured cells using an RNeasy Mini Kit (QIAGEN). cDNA was reverse transcribed from 1 μg of RNA using the iScript cDNA Synthesis Kit (Tiangen), and SYBR green–based real-time PCR was performed using the Mx3005p system (Stratagene). The primers used for NOS1 were forward: 5′-CAGAGGATGGCAGTCTGTTTC-3′; reverse: 5′-CTCAAGAGCACTGGATCTCAG-3′; and the primers for GAPDH were forward: 5′-GAACGGGAAGCTCACTGG-3′; reverse: 5′-GCCTGCTTCACCACCTTCT-3′ (Invitrogen).

Western blotting was performed using rabbit polyclonal anti-nNOS (Santa Cruz Biotechnology Inc.) at a 1:1,000 dilution and mouse mAb against GAPDH at a 1:5,000 dilution. Secondary antibodies used were peroxidase-conjugated anti-rabbit IgG and anti-mouse IgG (Bioss), respectively, at a 1:3,000 dilution. Blots were scanned, and immunoreactive bands were quantified using Quantity One Software (Bio-Rad). NOS signal intensities in silenced and control cells were normalized to GAPDH values.

*Gene expression profiling*. Total RNA from melanoma cell lines and patients' melanoma metastases was extracted using an miRNeasy Mini Kit (QIAGEN) (13). cDNAs were fragmented, biotinylated, and hybridized to the GeneChip Human Gene 1.0 ST Arrays (Affymetrix WT Terminal Labeling Kit). Expression data were normalized using the RMA algorithm (Partek Inc.). Data were $\log_2$ transformed for parametric analysis. All analyses were performed using the Partek Genomic Suite. Principal component analysis (PCA) was applied for visualization based on the complete dataset. Class comparison was based on ANOVA, encompassing variations related to batch effect and other hidden variables. Heatmaps are presented based on Partek visualization programs. The functional interpretation of gene signatures was executed using IPA 3.0 (http://www.ingenuity.com). Microarray data were deposited in the Gene Expression Omnibus (GEO) database (GEO GSE44851).

The RNA from 9 patients' PBMC samples was obtained from the University of Virginia Medical Center (14). Samples were labeled with Cy5 and mixed with a Cy3-labeled reference consisting of pooled PBMCs from 5 normal donors obtained from apheresis and hybridized to in-house–printed whole-genome human 36K oligo arrays, representing 25,100 unique human genes (Operon Human Genome Array-Ready Oligo Set, version 4.0). Gene expression values were displayed as $\log_2$-transformed fluorescence intensity ratios of red (samples) to green (PBMCs reference). Microarray data were deposited in the GEO database (GEO GSE32611).

*CGH assay and analysis*. Genomic DNA was isolated from the melanoma cell lines and PBMCs of a healthy female donor using the QIAamp DNA Mini Kit (QIAGEN), and 1.5 μg was fragmented, labeled, purified, and hybridized to Agilent $2 \times 10^5$ K arrays according to the Agilent Oligo Nucleotide Array–Based CGH for Genomic DNA Analysis (version 6.2.1) protocol. Data were extracted using Agilent's Feature Extraction Software. Copy number variation was measured according to the Partek Genomic Suite. After circular binary segmentation normalization, copy number gains and losses were detected using a hidden Markov model algorithm in the Partek copy number workflow for unpaired samples. Amplifications were defined as segments with $\log_2$ ratios greater than 0.15. Deletions were defined as segments with $\log_2$ ratios less than –0.3. Segments were defined as regions that differed from neighboring regions by at least 10 markers. The regions

identified were annotated using NCBI's RefSeq hg19. Microarray data were deposited in the GEO database (GEO GSE44850).

*Clinical samples*. Nine paired melanoma and PBMC samples were obtained from the Hematology Oncology unit at the University of Virginia Medical Center before IL-2 treatment. Patients were histologically confirmed as having metastatic malignant melanoma. Exclusion criteria included pregnancy, ischemic heart disease, brain metastasis, or requirement for corticosteroids (14).

Pretreatment snap-frozen tumor biopsies from 113 melanoma patients were obtained from the Surgery Branch of the NCI. These patients were treated under five consecutive phase II clinical trials for adoptive therapy of autologous TILs (15, 16). Response (CR, PR, or NR) was assessed using the RECIST guidelines starting approximately 4 weeks after TIL administration and at regular intervals thereafter. Among 113 patients, 24 achieved a durable CR (21%), 34 had a PR (30%), and 55 had NR (49%). A PR or NR was considered an overall noncomplete response (non-CR, PR+NR, 79%). See Supplemental Methods for more details.

*Statistics*. All data were tested for normality using the Kolmogorov-Smirnov test to decide whether parametric or nonparametric statistical tests were to be applied. Parametric unpaired tests included Pearson's product-moment correlation coefficient ($r$, correlation between two variables), an unpaired Student's $t$ test (comparison of two population means), and ANOVA (comparison of multiple population means). The corresponding nonparametric tests included Spearman's rank correlation coefficient ($\rho$), the Mann-Whitney $U$ test, and Kruskal-Wallis ANOVA, respectively. The Wilcoxon test was used to compare paired nonparametric data (e.g., flow cytometry PBMC p-STAT1 data paired according to the donor sources). A $\chi^2$ test was used to compare categorical variables. All tests were two-sided, and $P$ values of less than 0.05 were considered statistically significant.

*Study approval*. All human samples were obtained from clinical protocols approved by the IRB of the NCI or the University of Virginia Medical School and were considered relevant after receipt of written informed consent from all participants or their guardians.

## Acknowledgments

We thank David A. Wink (Radiation Biology Branch, NCI, NIH) and Harvey Klein (Department of Transfusion Medicine, Clinical Center and trans-NIH CHI, NIH) for their useful comments. D. Bedognetti's fellowship was supported by a 2011 Young Investigator Award from the Conquer Cancer Foundation of the American Society of Clinical Oncology. This work was supported by funds from the National Basic Research Program of China (973 Program 2010CB529406). The majority of this work was performed at the Infectious Disease and Immunogenetics Section (IDIS) of the Department of Transfusion Medicine, Clinical Center and trans-NIH Center for Human Immunology (CHI), NIH.

Received for publication March 14, 2013, and accepted in revised form January 22, 2014.

Address correspondence to: Qiuzhen Liu, Cancer Research Institute, Southern Medical University, Guangzhou, China. Phone: 01186.020.62789410; Fax: 01186.020.61648226; E-mail: liuqiuzhen@126.gov. Or to: Francesco M. Marincola, Office of the Chief, Research Branch, Sidra Medical and Research Centre, Al Nasr Tower, West Bay, Doha, Qatar. Phone: 974.7049.7777; Fax: 974.4404.7777; E-mail: fmarincola@sidra.org.

1. Critchley-Thorne RJ, Yan N, Nacu S, Weber J, Holmes SP, Lee PP. Down-regulation of the interferon signaling pathway in T lymphocytes from patients with metastatic melanoma. *PLoS Med*. 2007;4(5):e176.
2. Lesinski GB, et al. Multiparametric flow cytometric analysis of inter-patient variation in STAT1 phosphorylation following interferon Alfa immunotherapy. *J Natl Cancer Inst*. 2004;96(17):1331–1342.
3. Mortarini R, et al. Impaired STAT phosphorylation in T cells from melanoma patients in response to IL-2: association with clinical stage. *Clin Cancer Res*. 2009;15(12):4085–4094.
4. Critchley-Thorne RJ, et al. Impaired interferon signaling is a common immune defect in human cancer. *Proc Natl Acad Sci U S A*. 2009;106(22):9010–9015.
5. Simons DL, Lee G, Kirkwood JM, Lee PP. Interferon signaling patterns in peripheral blood lymphocytes may predict clinical outcome after high-dose interferon therapy in melanoma patients. *J Transl Med*. 2011;9:52.
6. Zimmerer JM, et al. Gene expression profiling reveals similarities between the in vitro and in vivo responses of immune effector cells to IFN-α. *Clin Cancer Res*. 2008;14(18):5900–5906.
7. Fridman WH, Pagès F, Sautès-Fridman C, Galon J. The immune contexture in human tumors: impact on clinical outcome. *Nat Rev Cancer*. 2012;12(4):298–306.
8. Ascierto ML, et al. An immunologic portrait of cancer. *J Transl Med*. 2011;9:146.
9. Lesinski GB, et al. Melanoma cells exhibit variable signal transducer and activator of transcription 1 phosphorylation and a reduced response to IFN-α compared with immune effector cells. *Clin Cancer Res*. 2007;13(17):5010–5019.
10. Thompson FH, et al. Cytogenetics of 158 patients with regional or disseminated melanoma. Subset analysis of near-diploid and simple karyotypes. *Cancer Genet Cytogenet*. 1995;83(2):93–104.
11. Jönsson G, et al. Genomic profiling of malignant melanoma using tiling-resolution arrayCGH. *Oncogene*. 2007;26(32):4738–4748.
12. Roschke AV, et al. Karyotypic complexity of the NCI-60 drug-screening panel. *Cancer Res*. 2003;63(24):8634–8647.
13. Spivey TL, et al. The stable traits of melanoma genetics: an alternative approach to target discovery. *BMC Genomics*. 2012;13:156.
14. Weiss G, et al. Molecular insights on the peripheral and intra-tumoral effects of systemic high dose rIL-2 (Aldesleukin) administration for the treatment of metastatic melanoma. *Clin Cancer Res*. 2011;17(23):7440–7450.
15. Dudley ME, et al. CD8+ enriched "young" tumor infiltrating lymphocytes can mediate regression of metastatic melanoma. *Clin Cancer Res*. 2010; 16(24):6122–6131.
16. Rosenberg SA, et al. Durable complete responses in heavily pretreated patients with metastatic melanoma using T-cell transfer immunotherapy. *Clin Cancer Res*. 2011;17(13):4550–4557.
17. Galon J, et al. The immune score as a new possible approach for the classification of cancer. *J Transl Med*. 2012;10:1.
18. Lloyd OC. Regression of malignant melanoma as a manifestation of a cellular immunity response. *Proc R Soc Med*. 1969;62(6):543–545.
19. Cochran AJ. Histology and prognosis in malignant melanoma. *J Pathol*. 1969;97(3):459–468.
20. Pages F, et al. Effector memory T cells, early metastasis, and survival in colorectal cancer. *N Engl J Med*. 2005;353(25):2654–2666.
21. Galon J, et al. Type, density, and location of immune cells within human colorectal tumors predict clinical outcome. *Science*. 2006;313(5795):1960–1964.
22. Tosolini M, et al. Clinical impact of different classes of infiltrating T cytotoxic and helper cells (Th1, th2, treg, th17) in patients with colorectal cancer. *Cancer Res*. 2011;71(4):1263–1271.
23. Wang E, Worschech A, Marincola FM. The immunologic constant of rejection. *Trends Immunol*. 2008;29(6):256–262.
24. Wang E, Tomei S, Marincola FM. Reflections upon human cancer immune responsiveness to T cell-based therapy. *Cancer Immunol Immunother*. 2012;61(6):761–770.
25. Wang E, Uccellini L, Marincola FM. A genetic inference on cancer immune responsiveness. *Oncoimmunology*. 2012;1(4):520–525.
26. Zea AH, et al. Alterations in T cell receptor and signal transduction molecules in melanoma patients. *Clin Cancer Res*. 1995;1(11):1327–1335.
27. Zea AH, et al. Arginase-producing myeloid suppressor cells in renal cell carcinoma patients: a mechanism of tumor evasion. *Cancer Res*. 2005; 65(8):3044–3048.
28. Lee PP, et al. Characterization of circulating T cells specific for tumor-associated antigens in melanoma patients. *Nat Med*. 1999;5(6):677–685.
29. Huber V, Filipazzi P, Iero M, Fais S, Rivoltini L. More insights into the immunosuppressive potential of tumor exosomes. *J Transl Med*. 2008;6:63.
30. Whiteside TL. Immune suppression in cancer: effects on immune cells, mechanisms and future therapeutic intervention. *Semin Cancer Biol*. 2006; 16(1):3–15.
31. Filipazzi P, Huber V, Rivoltini L. Phenotype, function and clinical implications of myeloid-derived suppressor cells in cancer patients. *Cancer Immunol Immunother*. 2012;61(2):255–263.
32. Whiteside TL, Schuler P, Schilling B. Induced and natural regulatory T cells in human cancer. *Expert Opin Biol Ther*. 2012;12(10):1383–1397.
33. Cormier JN, et al. Natural variation of the expression of HLA and endogenous antigen modulates CTL recognition in an in vitro melanoma model. *Int J Cancer*. 1999;80(5):781–790.
34. Sabatino M, et al. Conservation of a core of genetic alterations over a decade of recurrent melanoma supports the melanoma stem cell hypothesis. *Cancer Res*. 2008;68(1):122–131.
35. Sartor CI, Dziubinski ML, Yu CL, Jove R, Ethier SP. Role of epidermal growth factor receptor and

STAT-3 activation in autonomous proliferation of SUM-102PT human breast cancer cells. *Cancer Res*. 1997;57(5):978–987.
36. Cheng F, et al. A critical role for Stat3 signaling in immune tolerance. *Immunity*. 2003;19(3):425–436.
37. Ho HH, Ivashkiv LB. Role of STAT3 in type I interferon responses. Negative regulation of STAT1-dependent inflammatory gene activation. *J Biol Chem*. 2006;281(20):14111–14118.
38. Wang W, et al. Modulation of signal transducers and activators of transcription 1 and 3 signaling in melanoma by high-dose IFNα2b. *Clin Cancer Res*. 2007;13(5):1523–1531.
39. Atreya R, Neurath MF. Signaling molecules: the pathogenic role of the IL-6/STAT-3 trans signaling pathway in intestinal inflammation and in colonic cancer. *Curr Drug Targets*. 2008;9(5):369–374.
40. Glynn SA, et al. Increased NOS2 predicts poor survival in estrogen receptor-negative breast cancer patients. *J Clin Invest*. 2010;120(11):3843–3854.
41. Switzer CH, et al. Nitric oxide and protein phosphatase 2A provide novel therapeutic opportunities in ER-negative breast cancer. *Trends Pharmacol Sci*. 2011;32(11):644–651.
42. Pos Z, et al. Genomic scale analysis of racial impact on response to IFN-α. *Proc Natl Acad Sci U S A*. 2010;107(2):803–808.